

Chemical Analysis of the Superatom Model for Sulfur-Stabilized Gold Nanoparticles

Jeffrey R. Reimers,[†] Yun Wang,[†] Burak O. Cankurtaran,[‡] and Michael J. Ford[‡]

[†] School of Chemistry, The University of Sydney, Sydney NSW 2006, Australia

[‡] Institute for Nanoscale Technology, University of Technology, Sydney, P.O. Box 123, Broadway, New South Wales 2007, Australia

E-mail: reimers@chem.usyd.edu.au; Mike.Ford@uts.edu.au

RECEIVED DATE (to be automatically inserted after your manuscript is accepted if required according to the journal that you are submitting your paper to)

Abstract: The superatom model for nanoparticle structure is shown inadequate for the prediction of the thermodynamic stability of gold nanoparticles. The observed large HOMO-LUMO gaps for stable nanoparticles predicted by this model are, for sulfur-stabilized gold nanoparticles, attributed to covalent interactions of the metal with thiy l adsorbate radicals rather than ionic interactions with thiolate adsorbate ions, as is commonly presumed. In particular, gold adatoms in the stabilizing layer are shown to be of Au(0) nature, subtle but significantly different from the atoms of the gold core owing to the variations in the proportion of gold-gold and gold-sulfur links that form. These interactions explain the success of the superatom model in describing the electronic structure of both known and infor matory nanoparticle compositions. Nanoparticle reaction energies are, however, found not to correlate with the completion of superatom shells. Instead, local structural effects are found to dominate the chemistry and in particular the significantl y different chemical properties of gold nanoparticle and bulk surfaces.

These conclusions are drawn from density-functional-theory calculations for the $\text{Au}_{102}(\text{p-mercaptobenzoic acid})_{44}$ nanoparticle based on the X-ray structure (Jadzinsky *et al. Science* **2007**, 318, 430), as well calculations for the related $\text{Au}_{102}(\text{S}^{\bullet}\text{-CH}_3)_{44}$ nanoparticle, for the inner gold-cluster cores, for partially and overly reacted cores, and for Au(111) surface adsorbates.

1. Introduction

Gold nanoparticles are of significant current interest because of possible applications in biology, catalysis, and nanotechnology, with thiol-stabilized systems being of particular importance owing to their stability and ease of production.¹⁻³ Key structural information for gold nanoparticles was recently obtained from the X-ray diffraction results of Jadzinsky *et al.* with 1.1 Å resolution.⁴ They found that adatom-bound RS-Au-SR-type “staple” bonding motifs cover the surface of an Au_{79} core in the stable $\text{Au}_{102}(\text{SR})_{44}$ cluster; the stabilizing ligand SR used was S-C₆H₄-COOH derived from *p*-mercaptobenzoic acid (*p*-MBA), HSR. These units are oriented with their nearly collinear S-Au-S atoms almost parallel to the core surface and their organic groups pointing outwards. Figure 1 shows an analogous structure in which this complex adsorbate is replaced with the methanethiyl (MT) radical $\text{SR} = \text{SCH}_3$, maintaining the original RS-Au-RS head-group torsional angles; this modification allows the key structural features to be more easily visualized. The Au_{79} gold core is also shown in Figure 1 and has pseudo D_{5h} symmetry. So that its reactivity can be subsequently highlighted, we depict this in terms of 39 inner atoms (shown yellow) supplemented by 5 rings of gold atoms (shown brown) that form two polar caps and an equatorial ring. Attached to the Au_{79} gold core are 21 adatom-bound adsorbates made up of 19 RS-Au-SR units and two RS-Au-(RS)-Au-SR units, with the final cluster having C_2 symmetry. The 23 gold adatoms are shown in red in the figure, which provides views along the orthogonal C_2 and C_5 directions. Each RS-Au-SR or RS-Au-(RS)-Au-SR unit makes one bond to core gold atoms via each

terminal sulfur and typically two bonds to the core via each gold atom; the () indicates that this group does not interact directly with the core. Only the 39 inner atoms do not bond to sulfur, but of these 8 bond to gold atoms from the RS-Au-SR or RS-Au-(RS)-Au-SR units.

A significant known aspect of the structure of thiol-passivated gold clusters is the superatom model of electronic stability obtained from the jellium theory.⁵⁻⁷ This states that the number of available Au 6s electrons must be a ‘magic number’ such as 2, 8, 18, 34, 58, 92, or 138 obtained by filling shells quantized by angular momentum.⁷⁻⁹ In particular, a magic number of 58 electrons corresponds to the occupation $1s^2 1p^6 1d^{10} 2s^2 1f^{14} 2p^6 1g^{18}$ while 92 electrons arises from $1s^2 1p^6 1d^{10} 2s^2 1f^{14} 2p^6 1g^{18} 2d^{10} 3s^2 1h^{22}$; other structures such as $1s^2 1p^6 1d^{10} 2s^2 1f^{14} 2p^6$ with 40 electrons may also be stable.^{5,7} Gold 6s electrons are made unavailable by chemical bonding processes such as ionic and covalent bonding.⁷ For the $Au_{102}(SR)_{44}$ clusters considered, each of the 21 attached RS-Au-SR or RS-Au-(RS)-Au-SR units is interpreted as making unavailable one electron from the Au_{79} core, leaving 58 available electrons in accordance with the model prediction.⁷ Each RS-Au-SR or RS-Au-(RS)-Au-SR unit forms one link to the inner core via each terminal sulfur and typically two links per gold atom. The similar effect of RS-Au-SR and RS-Au-RS-Au-SR in making just one core electron unavailable is taken to indicate that the gold-adatom to gold-core interactions are too weak to influence the qualitative properties of the interaction.^{7,10,11} Indeed, the gold-adatom to gold-core interactions are presumed to be weak as “the gold atoms in the cluster are in two distinct chemical states: the 79 core Au atoms are in a metallic (charge neutral) state, whereas the 23 Au adatoms that belong to the $RS-Au(SR)_x$ oligomeric units are oxidized”;⁷ rather weak interactions (the aurophilic effect) are known between pairs of Au(I) atoms in small molecular complexes.¹²

Significant achievements of the superatom model include the prediction¹³ of the existence of another nanoparticle, $[Au_{25}(SR)_{18}]$, before it was observed.¹⁴ This cluster contains a magic number of 8 gold core electrons. However, stable $Au_{25}(SR)_{18}$ clusters with other oxidation states have also been

observed¹⁵ in which only 6 or 7 core electrons are present,^{13,16} with calculations predicting stable ions with charges ranging from -3 to +3. These results confirm that the superatom model correctly predicts the electronic structure of the clusters but the notion that particular stability is associated with superatom shell filling is not supported.¹⁷ Similarly, the assignment¹⁸ based on computational modeling of the structure of an observed 29 kDa cluster to Au₁₄₄(SR)₆₀, a cluster with a superatom core containing just 84 electrons, 8 short of the magic number 92, also questions whether or not there is a link between superatom-shell filling and chemical stability.

Here the chemical nature of the gold atoms in the cluster core and in adatom shell are determined, identifying the factors leading to the successes of the superatom model whilst identifying its inadequacies in predicting thermodynamic properties for simple model reactions of clusters. Density-functional-theory (DFT) calculations are performed using the generalized gradient approximation (GGA). The SIESTA program,^{19,20} with the GGA functional due to Perdew, Burke and Ernzerhof²¹ is used for calculations on large systems with SR = S[•]-C₆H₄-COOH and the VASP program,^{22,23} with the PW91 GGA functional²⁴ is used for the smaller S[•]-CH₃; all structures are fully optimized in vacuum. We consider the structure of 37 species and the energetics of 55 reactions between them. In addition, we focus on the differences observed between the chemistry of adsorption to the Au(111) surface by organic sulfur ligands and the properties of organic-sulfur stabilized nanoparticles. Chemisorption of organic sulfur ligands RS to the Au(111) crystal surface via gold adatoms is commonly,²⁵⁻³¹ but not universally,³² observed, with the controlling factors being a subtle balance of head-group and inter-adsorbate interactions. The nature of the adsorbate does not appear to be critical to nanoparticle formation, however.³³ We identify the features responsible for the differing chemical natures, leading to a more complete description of nanoparticle chemistry.

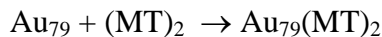
2. Results and Discussion

Details of all the nanoparticles considered and their chemical reactions are reported in Supporting Information, along with optimized structures for 30 important species. Test calculations using SIESTA for MT reveal no significant differences between the results of the (very different) SIESTA and VASP computational approaches: all energies differ by less than 0.2 eV per bond, an amount of order of the typical absolute accuracy of DFT, and an amount smaller than the differences subsequently used to make chemically significant conclusions. The results obtained for MT and *p*-MBA adsorbates are qualitatively similar, indicating that inter-adsorbate interactions do not provide the most significant forces leading to nanoparticle assembly; this is consistent with the picture of cluster structure obtained experimentally by varying the ligands.³³

2.1 Bare gold clusters. First we consider the gold atoms in the absence of their stabilizing adsorbate radicals. Of the total 102 gold atoms, 23 are raised above the surface of a continuous core of 79 atoms. Of these, 30 form polar caps while 10 form an equatorial ring around a symmetric Au₃₉ centre, as shown in Figure 1. Like most naked clusters of this size,³⁴ we predict the Au₃₉ centre, and the centre plus the equatorial ring, to be unstable with respect to low-symmetry distortions. In contrast, we find that Au₇₉ does form a stable local minimum. However, a much more stable reconstructed cluster, lower in energy by 3.9-4.2 eV (see Supporting Information) is also found. As shown in Figure 1, this reconstruction involves cluster elongation and insertion of the equatorial ring into the underlying surface. Hence we see that adsorbate attachment causes the gold core to take on quite a different structure than it would otherwise.

2.2 Chemical binding to the Au₇₉ core compared to Au(111). Chemical bonding to the Au₇₉ core can be considered as being directly analogous to the binding to surfaces of bulk gold, with in each case the competing possibilities of direct chemisorption and adatom-bound adsorbates. While calculations

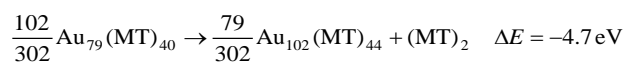
indicate that the disulfide of MT, CH_3SSCH_3 , binds dissociatively to flat Au(111) with $\Delta E = -0.60$ eV (using VASP and 0.78 eV using SIESTA, other values calculated using the same density functional include 0.78 eV³⁵ and 0.66 eV³⁶ after application of our calculated dimerization energy from Supporting Information), its binding to unreconstructed Au_{79}



is considerably more exothermic, $\Delta E = -1.3$ to -3.6 eV, depending on the adsorption site. Note that, while thiol reagents are most often used in nanoparticle-formation experiments and disulfide-bound clusters have not been observed as reaction products, we choose to consider the formation chemistry in terms of the associated disulfide reactions as these are reversible and could play a significant role in nanoparticle growth and rearrangement; all quoted energies may readily be converted to those for the reactions of adsorbate radicals or thiols, if desired. Addition of 20 disulfide molecules produces the highly symmetric D_{5h} cluster $\text{Au}_{79}(\text{RS})_{40}$ shown in Figure 1 with an average energy of adsorption per disulfide of $\Delta E = -1.08$ eV, indicating much stronger binding to this gold cluster than to the flat gold surface. Even after the energy required to construct the Au_{79} core from its optimal form (Figure 1) is removed, the binding $\Delta E = -0.88$ eV remains 50% more exothermic than that to the flat surface. This strong binding also occurs despite the large surface adsorbate density of $\text{Au}_{79}(\text{RS})_{40}$ of 5.3 sulfur atoms per nm^2 , significantly larger than the value of 4.4 nm^{-2} calculated by the same computational methods for MT above Au(111), see Table 1.

On Au(111), chemisorption to the flat surface and chemisorption via adatoms are finely balanced processes, with for MT $\Delta E = -0.60$ eV for the flat surface and -0.64 eV for adatom binding (when the adatom is mined from a step edge). This difference is sufficiently small to allow steric interactions between adsorbates to control the observed structure of thiol monolayers.^{32,37} For the nanoparticle, the variations in the energy with metal-adsorbate structure are much greater so that inter-adsorbate interactions become far less significant. To emphasise the importance of the head-group interactions,

we note that, despite the enhanced binding found to Au₇₉, the Au₇₉(MT)₄₀ cluster itself is calculated to be highly thermodynamically unstable compared to Au₁₀₂(MT)₄₄, with



A possible cause of the enhanced stability of Au₁₀₂(MT)₄₄ over Au₇₉(MT)₄₀ is its superatom-type electronic configuration. The calculated average energy of binding per gold atom of the reconstructed Au₇₉ cluster core is -2.57 eV, much less than that for bulk gold, -3.20 eV, but very similar to that for Au₁₀₂, -2.57 eV. Hence the exothermicity of the Au₇₉(MT)₄₀ to Au₁₀₂(MT)₄₄ conversion must indeed arise from enhanced adsorbate-gold interactions following the formation of the RS-Au-RS units. The average energies calculated for



are -1.85 and -2.14 eV for RS = MT and *p*-MBA, respectively, including the energies required to pull the 23 adatoms away from the surface of an optimized Au₁₀₂ cluster to make adatoms, calculated to be -16 eV by SIESTA and -19 eV by VASP. Hence the actual adsorbate-gold interactions are three times stronger for binding to adatoms compared to binding to the surface of Au₇₉.

Improved insight into the importance of the superatom effect is obtained by considering the binding of RS-Au-SR and RS-Au-RS-Au-RS molecules to Au₇₉ and to flat Au(111). Optimized in the gas phase, RS-Au-SR and RS-Au-RS-Au-RS show linear-type structures typical of small gold-containing molecules;¹² the calculated charge on the gold atom in MT-Au-MT is 0.16 *e*, typical of the small amount of polarization found in covalent complexes of gold and sulfur, as well as to observed and calculated polarizations for sulfur adsorbates on gold surfaces³⁸ and on Au₁₈ and larger nanoclusters.³³ In particular, the calculations give no indication of oxidation of Au(0), the most electronegative of all metal atoms, by the weakly oxidizing organic sulfur ligands.

Figure 2 shows the optimized structures for MT-Au-MT above the Au(111) surface and a typical configuration from the $\text{Au}_{102}(\text{MT})_{44}$ nanoparticle. The key difference is that the hexagonal nature of the Au(111) surface presents the two gold atoms that bridge to the adsorbate gold at a distance of $R = 2.96$ Å apart, while in the nanoparticle this distance is extended to 4.2 Å. Shown also in the figure is the interaction energy between MT-Au-MT and a model Au_4 cluster constrained to the same topology as found on the crystal and nanoparticle surfaces, plotted as a function of the bridge-atom separation R . The energy of this simplistic model system falls 0.5 eV as the flat-surface-like Au_4 structure is allowed to relax towards that found on the nanoparticle. A single RS-Au-SR or RS-Au-RS-Au-RS adsorbate to (unreconstructed) Au_{79} is bound with $\Delta E = -2.8$ to -3.7 eV per RSSR depending on adsorption site, with an average energy (excluding the reconstruction lift) of -2.67 eV for $\text{Au}_{102}(\text{MT})_{44}$ whereas the binding of MT-Au-MT above Au(111) is just -1.85 eV. It thus appears that the simplistic 4-atom local interaction model captures the critical features of the differing chemical reactivities of the Au_{79} cluster surface and the surface of Au(111). This includes the conservation of the Au(0) valence state for all gold atoms, as predicted by the full DFT calculations of both the surface adsorbates and the gold nanoparticles. While the Au_4 local-interaction model does not account for the changing reactivity with coverage and other significant factors that are implicated, it is clear that chemical factors not contained in the superatom model are critical to nanoparticle chemistry.

2.3 The superatom model and chemical thermodynamics. Of all the chemical structures considered thus far, only $\text{Au}_{102}(\text{RS})_{44}$ fulfils the requirements of the superatom model. Indeed, as shown in Table 1, it has a significant HOMO-LUMO gap of 0.55 eV (see also refs.^{7,11,39}), while that for say $\text{Au}_{79}(\text{MT})_{40}$ is small, 0.1 eV, in accord with model predictions. Four investigations are performed to see if *any* calculated thermodynamic property can be understood directly in terms of the superatom model.

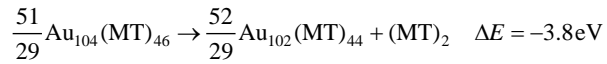
First, the nuclear and electronic structures are obtained for $[\text{Au}_{79}(\text{MT})_{40}]^-$, a cluster containing 40 available electrons. According to the jellium model this is a magic number if the $2p^6$ and $1g^{18}$ jellium bands do not overlap,⁴⁰ but unfortunately they are found to overlap for this cluster.

Next, we consider the effect on the binding energy of adding the same adsorbate pair to either a bare Au_{102} core to make $\text{Au}_{102}(\text{SR})_2$ or to $\text{Au}_{102}(\text{SR})_{42}$ to make $\text{Au}_{102}(\text{SR})_{44}$: in the second case the addition completes a superatom shell whereas in the first case it does not. For the configurations studied (see Supporting Information), the binding energies are calculated to differ by 0.02-0.22 eV depending on the ligand and its binding site. No profound connection thus exists between magic-number completion and binding energy.

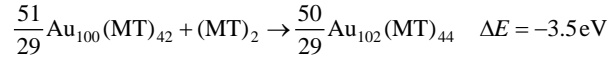
Third, we consider the effect of binding an adsorbate pair to Au_{80} , a structure obtained by adding a single appropriately placed gold adatom to the unreconstructed Au_{79} core-cluster (see Figure 1). We calculate ΔE of -4 to -6 eV depending on adsorbate and site, much more exothermic than for the parallel attachments to Au_{102} , ca. -2 eV. Hence the more gold atoms or adsorbate radicals that are added to Au_{79} , the more stable the structure becomes. This significant chemical effect occurs without completion of any special magic-number requirements.

Finally we consider the opposite situation and investigate chemical perturbations to $\text{Au}_{102}(\text{MT})_{44}$ that maintain the closed superatom shell through addition or removal of AuRS units. First, the structure $\text{Au}_{100}(\text{MT})_{42}$ is produced by symmetrically removing one terminal Au-SR from each of the two RS-Au-SR units, as shown in Figure 3. Second, the structure $\text{Au}_{104}(\text{MT})_{46}$ designed by Gao et al.³⁹ is investigated; this was made by adding Au-SR asymmetrically to existing RS-Au-SR units to fill small holes in the monolayer structure. We optimized this structure and the results are shown in Figure 4. It is known³⁹ to obey the 58-electron rule, and indeed our calculated HOMO-LUMO gaps after optimization remains quite large at 0.55 eV, see Table 1; we also calculate a large gap of 0.47 eV for

$\text{Au}_{100}(\text{MT})_{42}$. However, we find both nanoparticles to be highly thermodynamically unstable according to the reactions



and



The instability of $\text{Au}_{100}(\text{MT})_{42}$ follows directly from the energy of the bonds broken in its formation, with



As the size of the holes in the adsorbate coverage produced by removal of Au-MT is of the order of those that pre-exist at the polar caps (see Figures 1 and 3), chemical topology rather than coverage dominates this process. Significantly, however, we note that the differences here between this addition energy of -3.0 eV and the addition plus rearrangement energy of -3.5 eV for clusters obeying the magic number rules greatly exceeds the differences of 0.02-0.22 eV found earlier between chemical reactions that did/did not satisfy them.

Gao's $\text{Au}_{104}(\text{MT})_{46}$ structure after optimization does not display new bonds from each added sulfur to the Au_{79} core; instead, one added sulfur forms a disulfide bond with a neighboring adsorbate. This process is highlighted in Figure 4 where the two added Au atoms are shown in black, the disulfide is shown in green and the associated bond rearrangements are also sketched. Despite the presence of the weakly coordinated disulfide and the serious degradation of the thermodynamic cluster stability, the electronic structure of the cluster is not sufficiently perturbed to remove the band gaps and violate the 58-electron rule. Again the magic number rule is found to be poor for the prediction of specific chemical reaction properties. This result indicates that there exists a whole class of possible nanoparticles that obey superatom rules but are not observed experimentally.

To examine whether or not disulfide formation is key to the instability of $\text{Au}_{104}(\text{MT})_{46}$, a revised structure of C_2 symmetry was optimized following initial symmetrization of the top half of Gao et al.'s structure, and the results are also shown in Figure 4 and Table 1. The large HOMO-LUMO gap is maintained while the sulfur surface density is not excessive. The energy driving rearrangement to $\text{Au}_{102}(\text{MT})_{44}$, changes from -3.8 eV to -1.2 eV, however, indicating that this is a much more stable structure. Once again, binding strength and surface coverage are found to be more significant than fulfilling magic-number requirements.

2.4 How the band-gap is created on completion of the superatom shells. The principle by which the superatom criterion could lead to enhanced thermodynamic stability of nanoparticles is readily understood in terms of standard covalent and ionic bonding models- the total energy of the system is related to the sum of the occupied orbital energies, a quantity that is clearly minimized as a band gap is opened. Indeed, the perceived unavailability of gold core electrons is loosely associated with ionic and/or covalent bonding effects induced by the adsorbates.⁷ The calculated density of states of bare unreconstructed Au_{79} contains a block of 19 orbitals (2 more than that previously reported⁷) spanning the Fermi energy that have been assigned⁷ to the 2d, 3s, or 1h superatom-shells; these are occupied by 21 electrons. Figure 5 shows the energy of the alpha-spin orbitals of bare Au_{79} , along with the (unit) probability that these orbitals lie inside the Au_{79} core. Also shown in the figure are the energies of the orbitals of $\text{Au}_{102}(p\text{-MBA})_{44}$, along with the occupation probability obtained from the projection of each nanoparticle orbital onto the 19 Fermi-level spanning orbitals of bare Au_{79} . This displays what happens to these 19 orbitals as a result of chemical interaction with the 19 RS-Au-SR and two RA-Au-(RS)-Au-SR units that opens up a HOMO-LUMO gap in accordance with superatom-model predictions. Also shown in the figure is the integrated density of states showing the total number of the 19 bare Au_{79} orbitals distributed in the nanoparticle up to energy E .

Of the 19 2d-3s-1h-type orbitals of bare Au₇₉ that form the block spanning its Fermi-energy, in Au₁₀₂(*p*-MBA)₄₄ three appear very thinly distributed in the range -10 to -7 eV, three appear in a small peak at -6 eV so that the total alpha-spin occupation at the nanoparticle Fermi energy (-5.0 eV) is 6.4; nine orbitals also appear in a concentrated virtual band at -4.3 eV, and four more are moved to very high energies. In the nanoparticle, considerable mixing of these 19 bare-Au₇₉ orbitals with higher-energy unoccupied orbitals is also evident as the net charge on the Au₇₉ core of Au₁₀₂(*p*-MBA)₄₄ is just 0.04 per atom. Nevertheless, it is hence clear that the 19 2d-3s-1h-type orbitals are taken away from the Fermi energy not by sulfur oxidation but instead by covalent bonding effects. Indeed, the average charge of each S atom in the complex is just -0.24 (-0.20 total for each *p*-MBA ligand), indicating a thiyl rather than thiolate state, similar to calculated³⁸ and experiment⁴¹ results for sulfur-bound adsorbates to gold. The strength of the covalent bonding can be quantified by noting that the average energy change for the component of the 19 orbitals occupied in the nanoparticle is calculated to be -2.8 eV whilst that for the unoccupied component is 2.7 eV; the average value of the covalent interactions between the Au₇₉ core and the RS-Au-SR or RS-Au-(RS)-Au-SR units is thus 2.75 eV. This is in excellent agreement with the average energy for addition of RS-Au-RS to (unreconstructed) Au₇₉ of -2.67 eV reported earlier.

Valence rules provide a simple prescription for the determination of the number of core electrons that are bound covalently to the adsorbates using valences of S = -2, R = +1, and Au = +1. These rules give a valence of -1 to the RS-Au-RS and RS-Au-RS-Au-RS units, this predicting⁷ the observed removal of 21 electrons for Au₁₀₂(RS)₄₄. How this procedure can be mapped onto a purely covalent bond descriptors is not immediately obvious, however. For example, RS-Au-RS forms two Au-Au and two S-Au links to the core while RS-Au-RS-Au-RS forms four Au-Au and two S-Au links, with both types of links contributing significantly to the binding energy: the calculated energy of binding for RS-Au-RS (RS = MT) to the unreconstructed Au₇₉ core ranges between $\Delta E = -2.8$ to -3.7 eV depending on adsorption site while that for RS-Au-(RS)-Au-RS is much larger, -4.5 eV. Clearly, the Au-Au interactions contribute significantly to the binding, interactions typical of Au(0) chemistry that are

significantly stronger than the weak aurophilic interactions that typify Au(I) chemistry.¹² Significant insight into the valence rules used to predict superatom-shell filling is provided by the optimized structure of Gao et al.'s Au₁₀₄(RS)₄₆ structure (Figure 4).³⁹ The structure contains a physisorbed disulfide attached only to a gold adatom that clearly plays a minimal role in chemical bonding to the core and yet the HOMO-LUMO gap is maintained with all 21 electrons removed from near the Fermi energy. No scenario involving ionic bonding can account for this result whereas the covalent bonding scenario has no difficulties as the reconfigured (RSSR)-Au-Au-SR unit (see Fig. 4) still forms strong covalent bonds with the core.

A more detailed picture of the electronic structure of the Au₁₀₂(*p*-MBA)₄₄ nanoparticle is revealed in Figure 6 where the composition of each orbital in the vicinity of the Fermi energy is shown, analysed into contributions from the s, p, and d orbitals of the Au₇₉ core, the s, p, and d orbitals of the 23 Au adatoms, and, for convenience, just the p orbitals of the S atoms as well as those of C and O atoms. Also shown for these orbital types is the average occupancy per gold atom or per ligand $O(E) = \int_{-\infty}^E \rho(E') dE'$, where ρ is the average density of states, less that at the Fermi energy, $O(E_F)$. The ligands have a wide band gap, with their π and π^* bands commencing at -6.4 eV and -3.2 eV, respectively; the occupied gold d band starts at -6.5 eV with the onset of the unoccupied p block at high energy and not seen in the figure. However, each of these bands has a long tail that extends to include the HOMO and LUMO orbitals and up to 5 eV beyond, indicating a complex scenario of gold s-p-d hybridization as well as bonding and back-bonding interactions involving the gold and sulfur atoms. Per atom compared to the d¹⁰s¹ atomic configuration, the 79 gold core atoms have an average s charge of 0.12, p charge of -0.50, and d charge of 0.42 giving a net charge of 0.04, while for the 23 gold adatoms, these charges are 0.04 (s), -0.30 (p), 0.48 (d), and 0.22 (total). Hence the local chemical environment has a significant effect on the binding properties.

Most important is the description in Figure 6 of the orbitals within the ligand- π band gap. These are clearly of mixed origin, with each having 15-25 % sulfur p character. However, the HOMO and all occupied orbitals down to -5.4 eV, as well as the LUMO and all virtual orbitals up to -3.2 eV, have 60% net Au₇₉ core character and minimal Au adatom character. Figure 5 shows that the virtual orbitals in this block, including the LUMO, have Au₇₉-core character dominated by the 2d, 3s, and 1h superatom-orbitals⁷ found near the Fermi energy in bare Au₇₉, whereas the HOMO and nearby orbitals are characteristic of the lower-lying filled superatom shells. The result that the HOMO and LUMO are core-dominated is consistent with the observed and calculated results for [Au₂₅(SR)₁₈]⁻,^{13,15,16} but in contrast to calculations⁷ for Au₁₀₂(RS)₄₄ that counter-intuitively report oxidation and reduction involving ligand orbitals instead. The block of orbitals between -6.4 and -5.4 eV have over 50% ligand S, C, and O character and ca. 30% Au d character, mixed with ca. 5% Au adatom s character and 5% Au₇₉ 2d, 3s, and 1h superatom-model s character.

Finally, we consider the spread of energies over which the adatom and Au₇₉-core gold s orbitals are distributed in Figure 6. Strong covalent interactions with sulfur pushes the adatom s band down away from the Fermi energy, also manifesting Au s character down to -23 eV. Weaker interactions on average per gold atom of sulfur with the strongly interconnected Au₇₉ core result in the core orbitals significantly contributing to the HOMO, with those originating from the 2d-3s-1h superatom-model block of bare Au₇₉ mixing strongly with other core orbitals down to -10 eV; the Au₇₉-core s block extends down to only -13 eV. The gold adatoms and the gold core take quite different natures arising from the different chemical environments that these Au(0) atoms encounter.

3. Conclusions

The superatom model for nanoparticles is very successful in that it predicts significant features of observed nanoparticle structure. It is based on the identification of closed electron shells for the inner

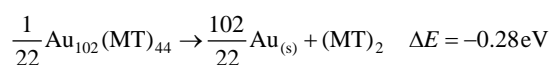
metallic core, with the closure demonstrated herein for sulfur-passivated gold nanoparticles to result from covalent bonding of this core with external adatom-bound organic adsorbates. This theory is attractive in that it directly parallels Pauling's valence theory for the structure of molecules. All results presented here and elsewhere indicate that this model predicts essential elements of the electronic structure of gold nanoparticles, evidenced perhaps most clearly by observed spectroscopic measurements. The key questions are: what are the causes of the effect, and what are the consequences for nanoparticle stability.

The cause of the effect is conventionally described in terms of the stark language of ionic bonding: the gold core is Au(0), the gold adatoms are in a different chemical state, Au(I), oxidized by the sulfur atoms during thiolate formation so that they interact with other gold atoms via only weak aurophilic interactions. However, the results from our, and indeed all other, DFT calculations are in stark contrast to this picture. The gold-sulfur bond is essentially covalent, the small differences in the electronegativity of gold (2.54) and sulfur (2.58) inducing only minor bond polarization. No evidence of thiolate or Au(I) formation is seen, the sulfur retaining thiyl form while the gold remains Au(0). The gold-sulfur bond is quite strong, however, so that the quantitative nature of the gold atoms is affected by its binding topology, i.e., the number of bonds it forms to sulfur and the number of bonds it forms to other gold atoms. As a result, the Au(0) adatoms develop an occupied s-band structure that is quite different from the metallic-gold-like Au(0) s-band structure of the Au₇₉ core; strong mixing is frequent when the core and adatom s bands overlap, reflecting interactions that are significant to binding energies but relatively too weak to control the actual band shape. Hence the s electrons from the adatoms need not be considered in defining the qualitative nature of the electronic structure of the core, resulting in the successes of the superatom model. Similarly, the RS-Au-RS and RS-Au-(RS)-Au-RS adatom complexes do not make core electrons unavailable at the Fermi energy by oxidation, as an ionic-bonding model requires, but rather through covalent bonding effects. Hence the structure of a nanoparticle can be changed without modifying the core electronic structure from the staple-type adatom motif RS-Au-

SR regularly observed to one in which some sulfur atoms attach via only physisorption to the adatoms (RSSR)-Au-Au-SR, a modification that would have a dramatic effect if core orbitals were instead made unavailable by oxidation.

For molecules, completion of closed electron shells is associated with large changes in thermodynamic properties such as reaction energies, with particular stability associated with the closed-shell structures, making this an essential starting point for the consideration of chemical processes. For nanoparticles, however, we find that the thermodynamic stability can be varied considerably without any obvious correlation with shell closure. Local chemical effects are found to control the chemical properties of the nanoparticle, not global core electronic structure properties. In particular, we find that the absorption of organic sulfur radicals to gold clusters is much more exothermic than the corresponding processes on gold surfaces, making the observed chemistries quite different in nature: this profound effect can be understood in terms of a simple frozen Au₄ cluster model of the local interactions.

Only thermodynamic stability has been investigated here and in previous experimental studies, owing largely to the enhanced difficulty of studying kinetic stability either computationally or experimentally. Pauling's valence rules for molecules not only explain thermodynamic stability but also explain kinetics- molecules with large band gaps have high-lying excited states that are difficult to access for chemical reactions. It is possible that the same effect applies to nanoparticles, with the band gap that is materialized in structures that obey the superatom model, combined with the known additional requirements of full surface coverage and surface-site passivation,⁷⁻⁹ leads to nanoparticles with high reaction barriers. That kinetic processes are of some significance is evidenced by the calculated reaction which indicates that the gold nanoparticles are in fact thermodynamically unstable with respect to decomposition into bulk gold and free disulfide molecules:



4. Methods

The SIESTA method implements DFT within a strictly localized pseudo-atomic basis^{19,20} for the valence and norm-conserving pseudopotential⁴² for the core electrons. Orbital confinement is specified using a single energy shift parameter, representing the raise in orbital energy due to confinement. Here we use a value of 5 mRy, which represents a good choice between well-converged total energies and computational effort.⁴³ The numerical basis sets, in all cases, are equivalent to double-zeta plus polarization and representing $5d^{10}6s^1$, $2s^22p^2$, $3s^23p^4$, $2s^22p^4$ valence electron structures for Au, C, S and O respectively. A scalar relativistic corrected pseudopotential is used in the case of Au. A real-space integration mesh equivalent to a plane-wave representation of 300 Ry is used, all geometry optimizations are performed to a tolerance of 0.04 eV/Å. While this is a relatively modest tolerance, further refinement only increases the computational time without changing the outcomes. We have previously tested all the present computational conditions and are confident they lead to well converged total energies and densities.⁴³

The Vienna *ab initio* simulation package (VASP)²² is employed to investigate the properties of $Au_n(MT)_n$ clusters with plane-wave bases, scalar relativistic ultrasoft pseudopotentials^{44,45} and a kinetic cutoff energy of 300 eV. The clusters are placed in a cubic box of $a = 40$ Å, and only the Gamma-point is used for the k -sampling. For the electron-electron exchange and correlation interactions, the functional of Perdew and Wang (PW91),²⁴ a form of the general gradient approximation (GGA), is used throughout. The broadening approach proposed by Methfessel and Paxton with an electronic temperature of 0.2 eV was used for the calculation of orbital occupancies. Calculations on gold surfaces were also performed using VASP using slabs 4-layers thick of the $6 \times \sqrt{3}$ Au(111) unit cell with a 2×6 surface k grid; the lowest layer of each slab was frozen at the optimized structure of bulk gold.

Acknowledgments. We thank the Australian Research Council for funding this research as well as National Computing Infrastructure (NCI) and the Australian Centre for Advanced Computing and Communications (AC3) for the provision of computer resources.

Supporting Information Available: Full details of the chemical reactions studied and optimized cluster coordinates. This material is available free of charge via the Internet at <http://pubs.acs.org>.

References

- (1) Daniel, M. C.; Astruc, D. *Chem. Rev.* **2004**, *104*, 293.
- (2) Hutchings, G. J.; Brust, M.; Schmidbaur, H. *Chem. Soc. Rev.* **2008**, *37*, 1759.
- (3) Ackerson, C. J.; Jadzinsky, P. D.; Kornberg, R. D. *J. Am. Chem. Soc.* **2005**, *127*, 6550.
- (4) Jadzinsky, P. D.; Calero, G.; Ackerson, C. J.; Bushnell, D. A.; Kornberg, R. D. *Science* **2007**, *318*, 430.
- (5) De Heer, W. A. *Rev. Mod. Phys.* **1993**, *65*, 611.
- (6) Zheng, J.; Nicovich, P. R.; Dickson, R. M. *Annu. Rev. Phys. Chem.* **2007**, *58*, 409.
- (7) Walter, M.; Akola, J.; Lopez-Acevedo, O.; Jadzinsky, P. D.; Calero, G.; Ackerson, C. J.; Whetten, R. L.; Grönbeck, H.; Häkkinen, H. *Proc. Natl. Acad. Sci. U. S. A.* **2008**, *105*, 9157.
- (8) Khanna, S. N.; Jena, P. *Phys. Rev. Lett.* **1992**, *69*, 1664.
- (9) Ball, P. *New Scientist* **2005**, *185*, 30.
- (10) Pei, Y.; Gao, Y.; Shao, N.; Zeng, X. C. *J. Am. Chem. Soc.* **2009**, *131*, 13619.
- (11) Li, Y.; Galli, G.; Gygi, F. *ACS Nano* **2008**, *2*, 1896.
- (12) Schmidbaur, H.; Schier, A. *Chem. Soc. Rev.* **2008**, *37*, 1931.
- (13) Akola, J.; Walter, M.; Whetten, R. L.; Häkkinen, H.; Grönbeck, H. *J. Am. Chem. Soc.* **2008**, *130*, 3756.
- (14) Aikens, C. M. *J. Phys. Chem. C* **2008**, *112*, 19797.
- (15) Zhu, M. Z.; Eckenhoff, W. T.; Pintauer, T.; Jin, R. C. *J. Phys. Chem. C* **2008**, *112*, 14221.
- (16) Iwasa, T.; Nobusada, K. *Chem. Phys. Lett.* **2007**, *441*, 268.
- (17) Negishi, Y.; Chaki, N. K.; Shichibu, Y.; Whetten, R. L.; Tsukuda, T. *J. Am. Chem. Soc.* **2007**, *129*, 11322.
- (18) Lopez-Acevedo, O.; Akola, J.; Whetten, R. L.; Grönbeck, H.; Häkkinen, H. *J. Phys. Chem. C* **2009**, *113*, 5035.
- (19) Ordejon, P.; Artacho, E.; Soler, J. M. *Phys. Rev. B* **1996**, *53*, 10441.
- (20) Soler, J. M.; Artacho, E.; Gale, J. D.; Garcia, A.; Junquera, J.; Ordejon, P.; Sanchez-Portal, D. *J. Phys.: Condens. Matter* **2002**, *14*, 2745.
- (21) Perdew, J. P.; Burke, W.; Ernzerhof, M. *Phys. Rev. Lett.* **1996**, *77*, 3965.
- (22) Kresse, G.; Hafner, J. *Phys. Rev. B* **1993**, *47*, RC558.
- (23) Kresse, G.; Furthmüller, J. *Comput. Mat. Sci.* **1996**, *6*, 15.

- (24) Perdew, J. P.; Wang, Y. *Phys. Rev. B* **1992**, *45*, 13244.
- (25) Kondoh, H.; Iwasaki, M.; Shimada, T.; Amemiya, K.; Yokoyama, T.; Ohta, T. *Phys. Rev. Lett.* **2003**, *90*, 066102.
- (26) Mazzaello, R.; Cossaro, A.; Verdini, A.; Rousseau, R.; Casalis, L.; Danisman, M. F.; Floreano, L.; Scandolo, S.; Morgante, A.; Scoles, G. *Phys. Rev. Lett.* **2007**, *98*, 16102.
- (27) Maksymovych, P.; Sorescu, D. C.; Yates, J. T., Jr. *Phys. Rev. Lett.* **2006**, *97*, 146103.
- (28) Wang, Y.; Hush, N. S.; Reimers, J. R. *J. Am. Chem. Soc.* **2007**, *129*, 14532.
- (29) Torres, E.; Blumenau, A. T.; Biedermann, P. U. *Phys. Rev. B* **2009**, *79*, 075440.
- (30) Wang, Y.; Chi, Q. J.; Hush, N. S.; Reimers, J. R.; Zhang, J. D.; Ulstrup, J. J. *Phys. Chem. C* **2009**, *113*, 19601.
- (31) Voznyy, O.; Dubowski, J. J.; Yates, J. T.; Maksymovych, P. *J. Am. Chem. Soc.* **2009**, *131*, 12989.
- (32) Wang, Y.; Hush, N. S.; Reimers, J. R. *J. Phys. Chem. C* **2007**, *111*, 10878.
- (33) Shichibu, Y.; Negishi, Y.; Tsunoyama, H.; Kanehara, M.; Teranishi, T.; Tsukuda, T. *Small* **2007**, *3*, 835.
- (34) Dong, Y.; Springborg, M. *J. Phys. Chem. C* **2007**, *111*, 12528.
- (35) Vargas, M. C.; Giannozzi, P.; Selloni, A.; Scoles, G. *J. Phys. Chem. B* **2001**, *105*, 9509.
- (36) Gottschalck, J.; Hammer, B. *J. Chem. Phys.* **2002**, *116*, 784.
- (37) Wang, Y.; Chi, Q.; Hush, N. S.; Reimers, J. R.; Zhang, J.; Ulstrup, J. J. *Phys. Chem. C* **2009**, *113*, 19601.
- (38) Bilic, A.; Reimers, J. R.; Hush, N. S. *J. Chem. Phys.* **2005**, *122*, 094708.
- (39) Gao, Y.; Shao, N.; Zeng, X. C. *ACS Nano* **2008**, *2*, 1497.
- (40) De Heer, W. A. *Rev. Mod. Phys.* **1993**, *65*, 611.
- (41) Azzam, W.; Wehner, B. I.; Fischer, R. A.; Terfort, A.; Wöll, C. *Langmuir* **2002**, *18*, 7766.
- (42) Troullier, N.; Martins, J. L. *Phys. Rev. B* **1991**, *43*, 1993.
- (43) Ford, M. J.; Hoft, R. C.; McDonagh, A. *J. Phys. Chem. B* **2005**, *109*, 20387.
- (44) Vanderbilt, D. *Phys. Rev. B* **1990**, *41*, 7892.
- (45) Kresse, G.; Hafner, J. *J. Phys. Condens. Matter* **1994**, *6*, 8245.

Table 1. Calculated surface density of sulfur atoms^a

cluster	density (nm ⁻²)	HOMO-LUMO gap (eV)
Au ₇₉ (MT) ₄₀	5.3	0.14
[Au ₇₉ (MT) ₄₀] ⁻	5.3	0.02
Au ₁₀₂ (<i>p</i> -MBA) ₄₄	4.9	0.51
Au ₁₀₀ (MT) ₄₂	4.7	0.47
Au ₁₀₂ (MT) ₄₄	4.9	0.55
Au ₁₀₄ (MT) ₄₆	4.9	0.55
Au(111) surface	4.4	0

^a based on the area of the surface that passes through the sulfur atoms.

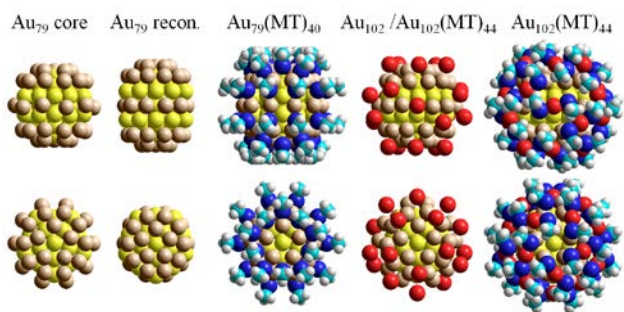


Figure 1. Atomic structures of nanoparticles and their components. Upper views- elevations looking down the C_2 axis; Lower views- plans looking down the pseudo- C_5 axis. Color code: carbon- cyan, hydrogen- white, sulfur- blue, Au_{39} center- yellow, Au polar caps and central ring- brown, Au adatom- red.

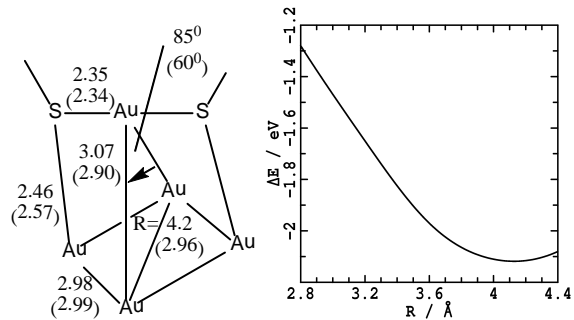


Figure 2. LEFT: extract of the optimized structure of an MT-Au-MT unit from $\text{Au}_{104}(\text{MT})_{46}$ is compared to that adsorbed above Au(111) (shown in parenthesis). RIGHT: the binding energy of MT-Au-MT to an Au_4 cluster similar to the base of these extracted structures is shown as a function of the central Au-Au bond length R .

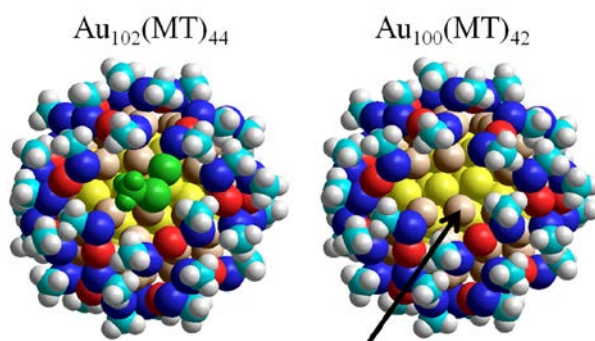


Figure 3. Effect of removing a ligand pair: Left- Optimized structure of $\text{Au}_{102}(\text{MT})_{44}$ with a MT-Au end group of an MT-Au-MT-Au-MT unit highlighted in green; Right- $\text{Au}_{100}(\text{MT})_{42}$ optimized structure following removal of the two terminal MT-Au groups, with the arrow indicating an unpassivated gold cap atom. Color code: carbon- cyan, hydrogen- white, sulfur- blue, Au_{39} core- yellow, Au caps and central ring- brown, Au adatom- red.

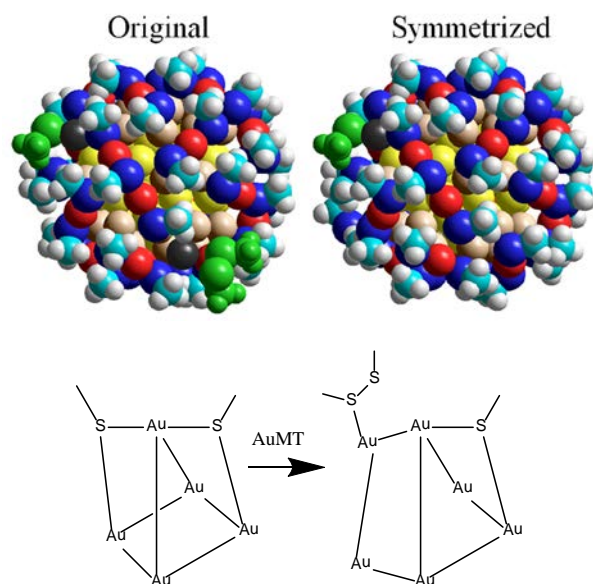


Figure 4. Effect of adding a ligand pair: TOP LEFT- Gao et al.'s optimized structure of $\text{Au}_{104}(\text{MT})_{46}$ with new MT-Au end groups added unsymmetrically to two MT-Au-MT units; TOP RIGHT- an alternate symmetrical structure; BOTTOM: atomic rearrangements for the reaction $\text{RS-Au-RS} + \text{AuRS} \rightarrow (\text{RSSR})\text{-Au-Au-SR}$ ($\text{SR}=\text{MT}=\text{SCH}_3$) on the nanoparticle leading to disulfide formation. Color code: carbon- cyan, hydrogen- white, sulfur- blue, Au_{39} core- yellow, Au caps and central ring- brown, Au adatom- red, newly added Au adatom- black. Under-coordinated SCH_3 groups and $(\text{SCH}_3)_2$ disulfide groups are highlighted in green.

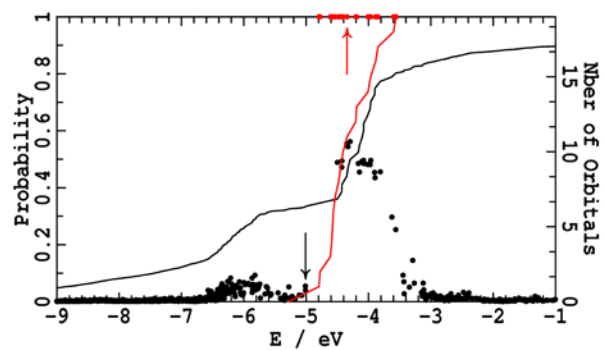


Figure 5. Band profiles at the Fermi energy as a function of orbital energy E : dots: the 19 alpha orbitals of bare unreconstructed Au_{79} that span its Fermi energy (red) and their redistribution in the $\text{Au}_{102}(\text{p-MBA})_{44}$ nanoparticle (black); lines: these distributions integrated to give the number of bare Au_{79} orbitals represented up to energy E . The arrows indicate the HOMO orbitals of each species.

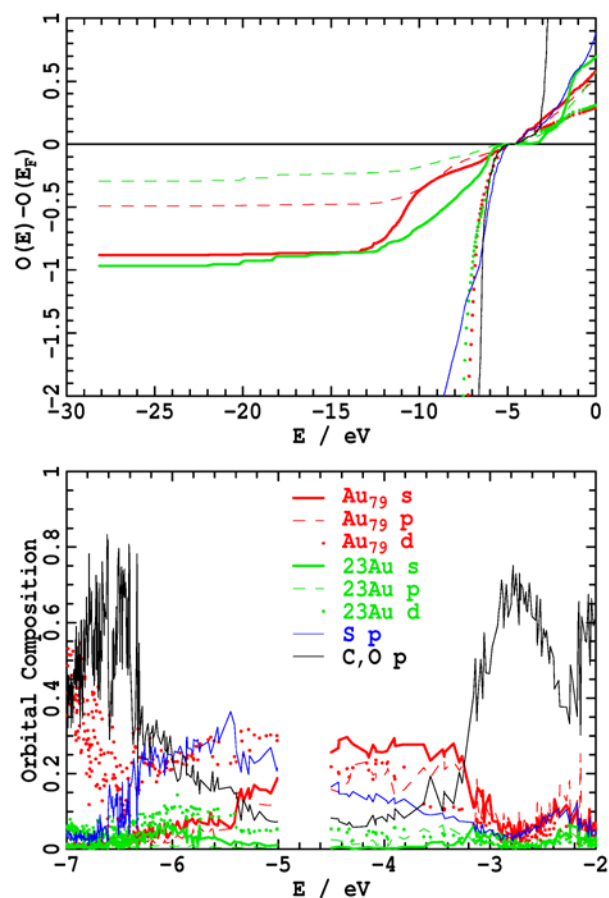


Figure 6. Lower: Composition of the occupied and virtual orbitals at energies E near the Fermi energy $E_F = -5.0$ eV of the $\text{Au}_{102}(\text{p-MBA})_{44}$ nanoparticle partitioned by Mulliken analysis into contributions from the Au_{79} -core's s, p and d orbitals, the 23 Au adatom's s, p, and d orbitals, the sulfur p orbitals, and the C and O p orbitals; Upper: for these bands, the integrated average number of occupied orbitals per atom or ligand $O(E)$ less that at the Fermi energy.

SYNOPSIS TOC

